Use of ^{10}Be to predict atmospheric ^{14}C variations during the Laschamp excursion : high sensitivity to cosmogenic isotope production calculations

Alexandre Cauquoin[a], Grant Raisbeck[b,a], Jean Jouzel[a], Didier Paillard[a]

[a] *Laboratoire des Sciences du Climat et de l'Environnement/Institut Pierre Simon Laplace (LSCE/IPSL CEA-CNRS-UVSQ), Orme des Merisiers, CEA Saclay, 91191 Gif-Sur-Yvette, France*

[b] *Centre de Spectrométrie Nucléaire et de Spectrométrie de Masse, IN2P3-CNRS-Université de Paris-Sud, Bât. 108, 91405 Orsay, France*

Ce chapitre est accepté dans *Radiocarbon*.

Ce chapitre s'intéresse à l'utilisation du ^{10}Be pour prédire les variations de ^{14}C atmosphérique durant l'excursion de Laschamp il y a ∼41 ka, ceci à l'aide d'un modèle océanique en boîtes simulant le cycle du carbone. L'objectif initial de cette étude était de d'estimer l'influence de cet événement sur le rapport ^{14}C/C * dans l'atmosphère entre 37,5 et 45,5 ka, déterminé à l'aide de mesures dans divers archives (spéléothèmes, coraux, sédiments marins). De plus, il était intéressant d'utiliser des données de ^{10}Be à haute résolution afin d'avoir accès au variations rapides du Δ^{14}C atmosphérique dû à la hausse de sensibilité de la production d'isotopes cosmogéniques à l'activité solaire durant l'excursion de Laschamp. Plusieurs étapes sont nécessaires pour obtenir les variations de Δ^{14}C à partir d'un enregistrement de ^{10}Be (voir section 2.2.2 et articles de Beer et al. [1988]; Bard et al. [1997]; Muscheler et al. [2004]; Nilsson et al. [2011]). En effet, après avoir corrigé la différence de sensibilité estimée entre la déposition polaire et globale de ^{10}Be, les données de ^{10}Be sont converties en ^{14}C à l'aide de calculs de production, puis entrées dans un modèle du cycle du carbone. Les calculs de production utilisés pour la conversion ^{10}Be – ^{14}C sont ceux de Masarik and Beer [2009] et la combinaison de ceux de Kovaltsov and Usoskin [2010] pour le ^{10}Be et de Kovaltsov et al. [2012] pour le ^{14}C. En comparant les amplitudes résultantes de Δ^{14}C atmosphérique avec ces deux calculs, nous avons finalement montré la forte sensibilité de cette méthode aux incertitudes liées aux calculs de production des isotopes cosmogéniques utilisés lors de la conversion du ^{10}Be en ^{14}C, en particulier durant les périodes de faible intensité du champ magnétique (telles que l'excursion de Laschamp).

∗. Dans la suite, la notation Δ^{14}C (variations par rapport au ratio ^{14}C/C actuel) sera couramment utilisée.

Abstract

The Laschamp excursion is a period of reduced geomagnetic field intensity occurring 40.7 ± 1.0 ky ago. As a consequence, cosmogenic isotope production increased dramatically and its sensitivity to solar activity was enhanced during this period. The latter occurs because a larger fraction of the lower-energy interstellar galactic cosmic-ray particles, normally excluded by the geomagnetic field, is able to reach the Earth's atmosphere. This produces a cosmogenic isotope production signal with a significant structure. As high-resolution ^{10}Be profiles from both Antarctica (EDC) and Greenland (NGRIP – GRIP) during this crucial are now available, one can use them as input into a box carbon cycle model in order to predict atmospheric ^{14}C variations due to the Laschamp excursion. For this purpose, ^{10}Be data are converted into ^{14}C, using production calculations for the ^{10}Be – ^{14}C conversion, after correction for the estimated difference of sensitivity between polar and global ^{10}Be deposition. Several scenarios of carbon cycle state are simulated, from pre-industrial to glacial conditions. Applying two recent cosmogenic isotope production calculations for the ^{10}Be to ^{14}C conversion, we found that the resulting atmospheric Δ^{14}C variations are very sensitive to which of these two are employed. For example, Δ^{14}C amplitude under glacial conditions varies from 260‰ (EDC) and 320‰ (Greenland) to 430‰ (EDC) and 510‰ (Greenland) depending on the formulation used for ^{10}Be – ^{14}C conversion.

Keywords: ^{10}Be, ^{14}C, Laschamp, geomagnetic field, cosmogenic production, ice core.

3.1 Introduction

Cosmogenic isotopes like ^{14}C and ^{10}Be are produced in the Earth's atmosphere mainly by interaction of Galactic Cosmic Rays (GCR) with nitrogen of the upper atmosphere. Since the GCR flux is modulated by the geomagnetic and heliomagnetic fields, records of ^{14}C and ^{10}Be provide useful information about variations in solar activity and geomagnetic field intensity in the past [Lal and Peters, 1967]. As a consequence, the higher the solar or geomagnetic field, the more primary cosmic ray particles are deflected, which leads to a decrease of cosmogenic isotope production.

^{14}C and ^{10}Be have been studied in natural archives for several decades. ^{14}C measurements were performed to establish ^{14}C calibration records because the ratio ^{14}C/^{12}C in the atmosphere has changed during the past due to variations of production (geomagnetic field intensity and solar activity) and modifications of the carbon cycle. Many such studies have been done in sediments [Hughen et al., 2004, 2006; Bronk Ramsey et al., 2012], speleothems [Beck et al., 2001; Hoffmann et al., 2010], corals [Fairbanks et al., 2005], and tree rings [Muscheler et al., 2008; Turney et al., 2010]. Calibration curves, regrouping all ^{14}C measurements, as IntCal04 and IntCal09 [Reimer et al., 2004, 2009] have been constructed for the conversion of radiocarbon ages to calibrated ages. ^{10}Be has been studied in ice cores from Antarctica [Yiou et al., 1985; Raisbeck et al., 1990, 1992; Horiuchi et al., 2008; Baroni et al., 2011] and Greenland [Beer et al., 1990; Finkel and Nishiizumi, 1997; Yiou et al., 1997; Wagner et al., 2001; Muscheler et al., 2004, 2005], as well as in sediments [Raisbeck et al., 1985; Robinson et al., 1995; Frank et al., 1997; Ménabréaz et al., 2011; Nilsson et al., 2011]. One advantage of ice cores is that they offer a relatively simple way to calculate ^{10}Be fluxes (from the measured concentration ^{10}Be and the estimated accumulation rate). Moreover, their higher resolution can be helpful for the study of shorter events due to solar activity for example.

Although ^{14}C and ^{10}Be are both produced by cosmic rays, their behaviors differ in the atmosphere. Indeed, ^{10}Be atoms become fixed to aerosols and are deposited very quickly after their production (within ∼1-2 years according to Raisbeck et al. [1981a]) whereas the ^{14}C atom is oxidized to CO_2 and enters in the global carbon cycle in which it is homogenized with stable carbon. As a consequence, ^{14}C concentration variations in different reservoirs are smoothed and delayed with respect to ^{14}C production variations. Masarik and Beer [1999] found that the stratosphere contributes 56% of the global production of ^{10}Be and Heikkilä et al. [2009] determined with their model that the stratospheric fraction of the total production is 65%. While most ^{10}Be produced in the troposphere is deposited near the latitude band in which it is formed, even the dominant proportion coming from the stratosphere probably does not have the time to be completely well-mixed because of its relatively short residence time compared to the mixing time of the air in the stratosphere. According to Field et al. [2006], the polar flux is about 20% less sensitive to variations of geomagnetic field intensity (and 20% more sensitive to variations of solar activity) than the global production. This fact will be taken into account for the ^{10}Be – ^{14}C conversion (see section 3.2.2).

Past ^{14}C production rate has been already studied using numerical models. Past changes of atmospheric ^{14}C concentration were, in most cases, simulated using geomagnetic intensity records retrieved from oceanic sediments (like NAPIS-75 [Laj et al., 2002] or GLOPIS-75 [Laj et al., 2004]). The geomagnetic intensity signal was converted into ^{14}C production with the help of calculations from Masarik and Beer [1999] (equations in Wagner et al. [2000]). These model results can be compared with reconstructed Δ^{14}C values obtained from well-dated archives like sediment records [Hughen et al., 2004, 2006] or speleothems [Beck et al., 2001; Hoffmann et al., 2010]. Recently, Hoffmann et al. [2010] used this method with GLOPIS-75 but converting it with an approximation from Elsasser [1956] (see section 3.2.3) instead of numerical values from Masarik and Beer [1999]. We will show here that the choice of production calculations can have huge consequences on the simulated atmospheric Δ^{14}C. As for ^{10}Be records, Bard et al. [1997], using the same approach as Beer et al. [1988], compared ^{10}Be-based ^{14}C (modelled from the South Pole record of Raisbeck et al. [1990]) with tree ring ^{14}C records to document how solar modulation has influenced the cosmonuclide production variations during the last millennium. Muscheler et al. [2004] used a model with a ^{10}Be composite record from GRIP and GISP2 (Greenland) as an input to compare it with Δ^{14}C from different sources, especially during the last 25 ky. Nilsson et al. [2011] also studied atmospheric Δ^{14}C adopting the same model but with the ^{10}Be GRIP record on the GICC05 time scale between 50 and 25 kyr BP.

Hereafter, we focus on the period around the Laschamp excursion. There has been considerable discussion about the magnitude and origin of high-level atmospheric Δ^{14}C measured in different archives at the time of this event. The Laschamp excursion represents a well-constrained geochronological event and has been dated at 40.7 $\pm$ 1.0 ky ago by Singer et al. [2009]. During this event, the geomagnetic field intensity was extremely weak (around 10% of present intensity). This had the effect to increase sharply cosmogenic isotope production (such as ^{10}Be and ^{14}C) [Raisbeck et al., 2007]. Moreover, cosmogenic isotope production was affected by an increased sensitivity to solar activity during this event. Indeed, a larger fraction of the lower energy interstellar galactic cosmic ray particles, normally excluded by the geomagnetic field, was able to reach the Earth's atmosphere. For example, Wagner et al. [2001] show that a 205 yr cycle, assumed to be of solar origin, was enhanced in the GRIP ^{10}Be record during the Laschamp excursion. High-resolution ^{10}Be profiles, with considerable structure, from both Antarctica (EDC, Raisbeck et al. [2007]) and Greenland (NGRIP – GRIP, Yiou et al. [1997]; Raisbeck et al. [2007], in preparation) during this period being now available, it was interesting to use them as input of a box carbon cycle model to predict the resulting atmospheric Δ^{14}C amplitude linked to the Laschamp excursion. For this, ^{10}Be data need to be converted into ^{14}C production. We will show that this step is crucial to determine the amplitude of atmospheric Δ^{14}C during this time. Indeed, new calculations of ^{14}C production from Kovaltsov et al. [2012] combined with those from Kovaltsov and Usoskin [2010] for ^{10}Be production calculations lead to a discrepancy in the resulting atmospheric Δ^{14}C amplitude for low geomagnetic field intensity (as the Laschamp excursion) compared with those of Masarik and Beer [2009] (see sections 3.2.2 and 3.4.1).

3.2 Modeling

3.2.1 ^{10}Be records from Greenland and EPICA Dome C

Three records were exploited for this analysis: one from the Antarctic plateau and two from Greenland, plus the geomagnetic field intensity GLOPIS-75 record (see section 3.2.3). One of the advantages of using ^{10}Be from ice cores is the high resolution which permits to take into account the structure of the cosmogenic production peak due to increased sensitivity to solar activity. The Antarctic record is EPICA Dome C [Raisbeck et al., 2007] and its time resolution is around 10 years between 37.5 and 45.5 ky BP (kiloyear Before Present) age range. EDC (75°06' S, 123°21' E) has been synchronized [Raisbeck et al., in preparation] to the North GRIP (NGRIP) time scale GICC05 [Svensson et al., 2008] between 40.4 and 42.1 ky BP using the Match protocol from Lisiecki and Lisiecki [2002]. The NGRIP record (75.1°N, 42.3°W) has an average time resolution of ∼7 years in the time range 40424-42040 yr BP. In order to have a more extended (37.5 – 45.5 ky BP) Greenland input for the model, we complemented the NGRIP record with the GRIP record (72.5°N, 37.3°W), which has a time resolution from ∼30-50 years [Yiou et al., 1997; Raisbeck et al., 2007], for the rest of the time scale. The two Greenland ice core records were placed on the GICC05 time scale [Svensson et al., 2008] and were normalized to the same average value over their common age range. To study production variations in ice cores, especially during periods of variable climate, it is probably better to use

^{10}Be flux instead of concentrations because ^{10}Be concentration is influenced not only by production variations but also by the amount of precipitation at the site. Assuming that ^{10}Be falls mainly by dry deposition on the Antarctic plateau [Yiou et al., 1985; Raisbeck et al., 1992], we can minimize the climatic component (precipitation) of the EDC record by calculating ^{10}Be flux, which is the product of the measured concentrations and the estimated accumulation rates [Raisbeck et al., 1992]. The ^{10}Be GRIP flux was calculated using the ss09sea accumulation rate [Johnsen et al., 2001]. The Greenland and EDC records are reported in Fig. 3.1b and 3.1c respectively. The GLOPIS-75 record [Laj et al., 2004] is also displayed for comparison in Fig. 3.1a. The high-pass filtered ^{10}Be flux of each record (cutoff frequency = 1/2000 years^{-1}), representing variations of production dominated by solar activity, is shown in Fig. 3.1d and 3.1e.

The EDC and Greenland records are different in several aspects. For EDC, the assumption that ^{10}Be falls by dry deposition is probably reasonable because this is a very dry region with an extremely low and relatively stable accumulation rate [EPICA, 2004]. Greenland is not as dry as the Antarctic plateau and the snow accumulation rate is more variable. It is important to keep in mind that calculated ^{10}Be fluxes are directly affected by uncertainties in the estimated accumulation rate of the studied sites. Moreover, the Greenland record has some additional limitations like the uncertainties about the ^{10}Be GRIP record (resolution, missing samples, corrections for filtered samples, Yiou et al. [1997]; Raisbeck et al. [2007]), and its combination with NGRIP.

3.2.2 Reconstruction of ^{14}C production from ^{10}Be flux

To calculate the ^{14}C production rate from the ^{10}Be flux, we assume that long-term variations ($\geqslant$ 2000 years) are due to fluctuations of the geomagnetic field intensity and variations on shorter time scales correspond to changes in solar activity [Muscheler et al., 2005]. To make this separation (Fig 3.1: bold curves), we used the AnalySeries program from Paillard et al. [1996]. First a correction to take into account the latitudinal dependency of ^{10}Be deposition is applied because, contrary to ^{14}C, ^{10}Be is probably not completely homogenized before its deposition in polar regions. Contributions from different regions to the flux of ^{10}Be deposited in polar regions have been estimated by comparisons of calculated ^{10}Be production from changes in geomagnetic field intensity with ^{10}Be records. Using the Vostok ice core, Mazaud et al. [1994] deduced that 25% of ^{10}Be was locally produced and 75% was modulated by global geomagnetic intensity changes. More recently, by the use of model-derived estimates, Field et al. [2006] found that polar deposition in

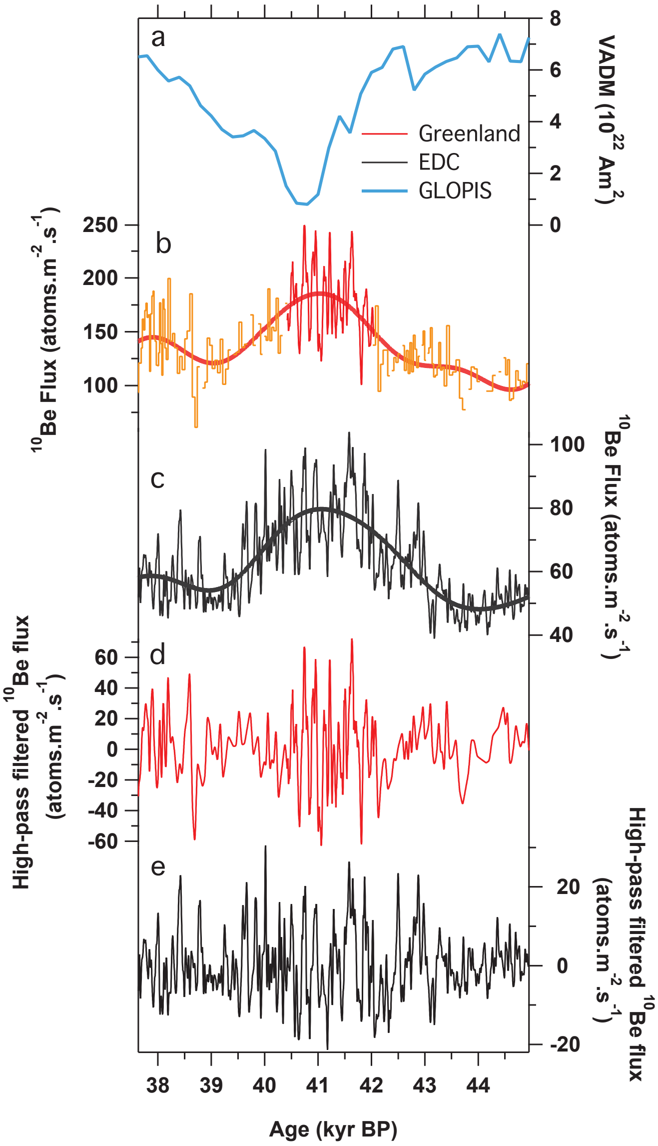

Figure 3.1: (a) GLOPIS-75 record [Laj et al., 2004] (b, c) ^{10}Be flux measured in the Greenland (red) and EDC (black) ice cores between 37.5 and 45.5 ky BP. EDC has been synchronized with NGRIP between 40 and 42 ky BP on GICC05 age scale. The Greenland record is a combination of NGRIP (thin red line) and GRIP (orange cityscape) data. The NGRIP record covers the time range 40424-42040 yr BP while the GRIP data are used over the rest of the time scale. The GRIP data were scaled in such a way that GRIP and NGRIP fluxes have the same average value over their common age range. The bold curves show the data after low-pass filtering (cutoff frequency = 1/2000 years^{-1}) assumed to be the geomagnetic component. (d, e) ^{10}Be flux in the Greenland (red) and EDC (black) ice cores after removing the low past component given by the bold curves in b and c, describing variations due to solar activity.

both hemispheres is enhanced by a factor of 1.2 (compared with global deposition) for solar activity induced variations and reduced by a factor 0.8 for geomagnetic intensity variations. We used these results in order to estimate the global ^{10}Be flux (see section 3.1). In contrast to Field et al. [2006], Heikkilä et al. [2008], using the ECHAM5-HAM General Circulation Model, found no indication of a polar enhancement. Indeed, they found a ^{10}Be "well-mixed" in the stratosphere which is sufficient to mask a latitudinal dependence in the polar regions [Heikkilä et al., 2009]. Muscheler et al. [2004] and Nilsson et al. [2011] assumed that the ^{10}Be flux from Greenland they used for Δ^{14}C modeling was an indicator of changes in global ^{10}Be production. Using this last hypothesis for our input and our carbon cycle model would decrease the atmospheric Δ^{14}C amplitude modelled by 30 – 60‰ depending on the ^{10}Be – ^{14}C conversion used (see chapter below and section 3.4.1).

After applying these corrections to ^{10}Be, we account for difference in production processes between ^{10}Be and ^{14}C. ^{14}C is produced by absorption of thermal neutrons while ^{10}Be is produced by spallation reaction (mainly with high energy neutrons) [Masarik and Beer, 1999, 2009]. Expressions in the article of Wagner et al. [2000] (using the results of Masarik and Beer [1999]) were previously used by Muscheler et al. [2004] or Nilsson et al. [2011] for ^{10}Be – ^{14}C conversion, and also by others [Laj et al., 2002; Hughen et al., 2004, 2006] to calculate the ^{14}C production rate from geomagnetic intensity record (see §4 of section 3.1). An update of these calculations has been released by Masarik and Beer [2009]. To our knowledge, it has not yet been applied for this type of study. Very recently, Kovaltsov et al. [2012] simulated ^{14}C production after having calculated ^{10}Be production variations according to geomagnetic field intensity and solar activity [Kovaltsov and Usoskin, 2010]. For convenience, the ^{10}Be – ^{14}C calculations of Kovaltsov and Usoskin [2010] and Kovaltsov et al. [2012] will be called KOV. Results of these two sets of calculations are shown as a function of the geomagnetic field intensity (B, relative to the present value) in Fig. 3.2. As can be seen, the predictions of relative ^{10}Be at low geomagnetic intensity, as well as the slope of the ^{14}C/^{10}Be production ratio as a function of the geomagnetic field intensity are very different for these two theoretical models. This has great consequences on the resulting atmospheric Δ^{14}C amplitude due to weak geomagnetic shielding during the Laschamp excursion (see section 3.4.1). Assuming that solar activity was on average constant during the studied period (solar modulation potential $\phi = 550$ MV according to the definition of Castagnoli and Lal [1980]), the sensitivity difference of ^{10}Be and ^{14}C to solar activity as a function of geomagnetic field intensity is also taken into account for shorter-term changes (less than 2000 years). The difference in the definition of the Local Interstellar Spectrum

(LIS) used by Masarik and Beer [2009] and KOV [Kovaltsov and Usoskin, 2010; Kovaltsov et al., 2012] is taken into account using the relation in the appendix of Usoskin et al. [2005]. We have also shown in Fig. 3.2a the approximation from Elsasser [1956] used by Hoffmann et al. [2010] to convert the GLOPIS-75 geomagnetic intensity record [Laj et al., 2004] into ^{14}C production. The consequences of the choice of Hoffmann et al. [2010] on simulated atmospheric Δ^{14}C is discussed below in section 3.2.3.

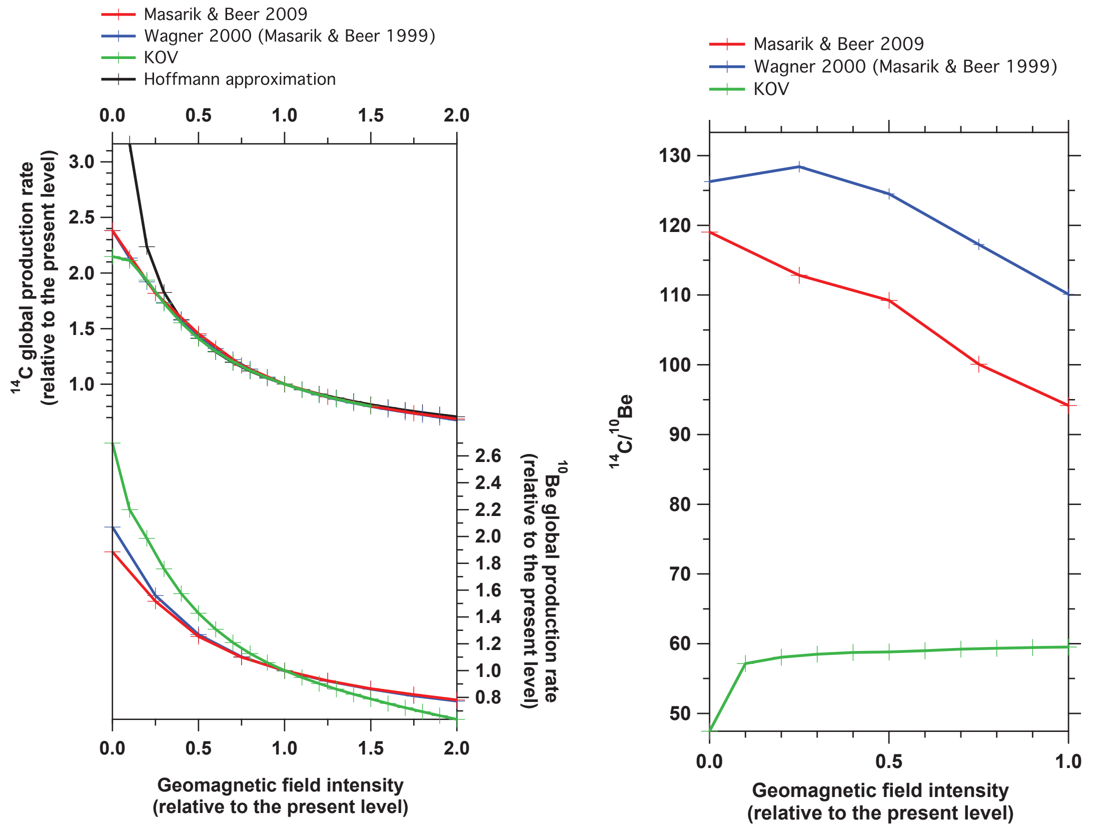

(a) (b)

Figure 3.2: (a) Dependence of predicted relative ^{14}C and ^{10}Be global production rate on geomagnetic field intensity for the solar modulation parameter $\phi = 550$ MV (based on the definition of Castagnoli and Lal [1980]). The blue curves are the production rates according to Wagner et al. [2000] [Masarik and Beer, 1999], the red curves represent the update from Masarik and Beer [2009], and the green curves come from the calculations of Kovaltsov and Usoskin [2010] for ^{10}Be and Kovaltsov et al. [2012] for ^{14}C. The black curve of ^{14}C global production rate corresponds to the approximation used by Hoffmann et al. [2010]. (b) ^{14}C/^{10}Be production rate ratio as a function of geomagnetic field intensity according to Masarik and Beer [1999] (blue), Masarik and Beer [2009] (red) and the KOV simulation (Kovaltsov and Usoskin [2010], Kovaltsov et al. [2012], green).

3.2.3 Approximation from Hoffmann et al. [2010]

Hoffmann et al. [2010] simulated atmospheric $\Delta^{14}C$ from 45 to 28 ky BP with the GLOPIS-75 geomagnetic intensity record [Laj et al., 2004] as input and found an amplitude of 550‰ which is consistent with their ^{14}C measurements from a speleothem. This type of simulation has been previously done by Laj et al. [2002] or Hughen et al. [2004, 2006] with more simple carbon cycle models. Unlike Hoffmann et al. [2010], they did not find such a large amplitude. The major difference between the simulation of Hoffmann et al. [2010] and the others is not so much the complexity of the carbon cycle model employed, but the use of the following approximation $P/P_0 = \sqrt{\frac{1}{M/M_0}}$ from Elsasser [1956] (with P the time-varying ^{14}C production rate, P_0 the present-day production rate, M the time-varying global geomagnetic intensity and M_0 the present geomagnetic intensity) instead of the relationship of Wagner et al. [2000] or Masarik and Beer [2009] (e.g. Fig. 3.2a) for the production input. To illustrate this point we show in Fig. 3.3 how the GLOPIS-75 geomagnetic intensity record is converted into relative global ^{14}C production rate using either the Masarik and Beer [2009] values (red), the KOV calculations (in green, Kovaltsov et al. [2012]), or the Hoffmann et al. [2010] approximation (black). The impact of this approximation can be seen when the geomagnetic field intensity is low (curve b on Fig. 3.3). Indeed, the maximum ^{14}C production rate rises by a factor of 2.13 and 2.08 with Masarik and Beer [2009] and Kovaltsov et al. [2012] formulas respectively, while it increases by a factor of 3.16 with the approximation. Indeed, because the geomagnetic intensity was less than 20% of its present value during the Laschamp excursion, the use of this approximation for this period [Hoffmann et al., 2010] is not appropriate. We can conclude that this approximation has a large effect of amplification on the ^{14}C production rate signal, thus on the simulated atmospheric $\Delta^{14}C$.

We used the three production-rate curves shown in the Fig. 3.3 as input to the carbon cycle model (presented in the following section 3.2.4) in order to see the consequences on modelled atmospheric $\Delta^{14}C$ (bottom of Fig. 3.3). The difference between the formula employed by Hoffmann et al. [2010] and the others is large: around 150‰ compared to Masarik and Beer [2009] or Kovaltsov et al. [2012] formulations. This means that the 550‰ amplitude found by Hoffmann et al. [2010] is partly an artefact due to this approximation, showing the importance of the formulas used to make the conversion from geomagnetic intensity into global ^{14}C production rate. In comparison, previous simulations made by Laj et al. [2002] or Hughen et al. [2004, 2006], who worked with geomagnetic records and the Masarik and Beer [1999] conversion (very similar to Masarik and Beer [2009] for ^{14}C pro-

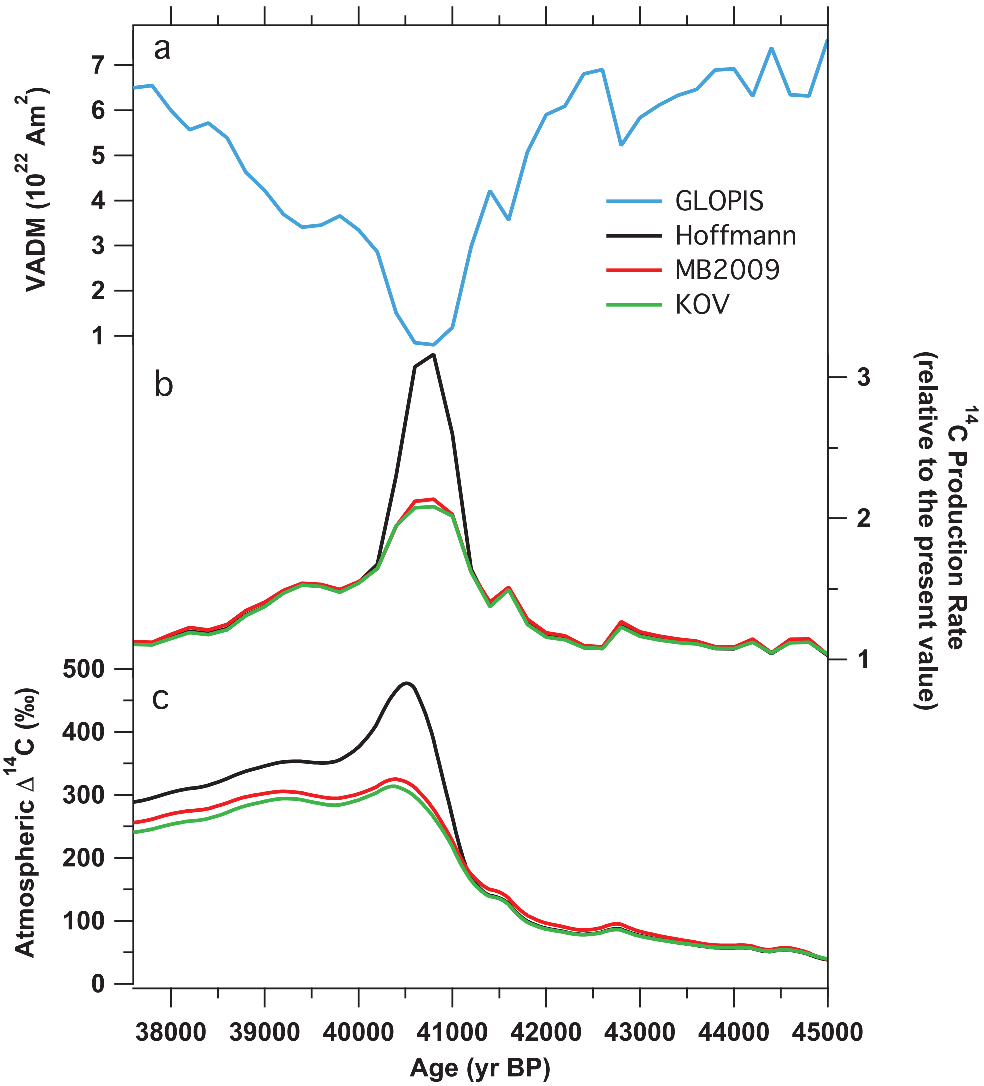

Figure 3.3: (a) GLOPIS-75 record [Laj et al., 2004]. (b) Comparison between converted ^{14}C production from GLOPIS-75 record with Hoffmann et al. [2010] approximation (black), Masarik and Beer [2009] update (red) and Kovaltsov et al. [2012] simulation (green). (c) Atmospheric Δ^{14}C obtained from production records in (b) with the 12 box-model. The differences in amplitude between the Hoffmann et al. [2010] approximation and the different global ^{14}C production calculations are around 150‰ with Masarik and Beer [2009] and Kovaltsov et al. [2012] formulations.

duction, e.g. Fig. 3.2a) as input of their model, found an amplitude of ∼300‰ and more than 200‰ respectively for pre-industrial conditions (see section 3.2.5). This is in good agreement with the amplitude of 290‰ simulated with our carbon cycle model using GLOPIS-75 and the equation from Masarik and Beer [2009] (see red curve on Fig. 3.3c), showing that our carbon cycle model gives results coherent with previous studies. We note that these results using Masarik and Beer [2009] and KOV calculations are smaller than $\Delta^{14}C$ amplitude from IntCal09 of Reimer et al. [2009] (e.g. Fig. 3.7, more than 450‰).

In addition to the reasons discussed in section 3.1, the use of ^{10}Be flux records in ice core has two advantages compared to geomagnetic intensity record in sedimentary cores: they have a higher resolution allowing the study of solar activity, and there is expected to be less uncertainty in the ice accumulation rate compared to that of sediments, and thus a more reliable chronology for duration of short term events such as the Laschamp excursion.

3.2.4 Description of the carbon cycle model

In order to investigate the influence of Laschamp event on atmospheric $\Delta^{14}C$, we used a 10-box ocean model (plus an atmosphere-box and a biosphere-box) made with the BoxKit2 program [Paillard, 1995] to simulate the carbon cycle (Fig. 3.4). This program was already used by [Laj et al., 2002] for their model with 17 boxes but no biosphere. The advantage of BoxKit2 is its flexibility: it is easy to vary the volume and areas of boxes, or the values of fluxes. To build our carbon cycle model, we were inspired by PANDORA [Broecker and Peng, 1986] and other models from Siegenthaler et al. [1980]; Bard et al. [1997]; Laj et al. [2002]; Hughen et al. [2004]. There exist several results of global average production rate for ^{10}Be and ^{14}C at present conditions (Webber and Higbie [2003], Kovaltsov and Usoskin [2010] for ^{10}Be, Kovaltsov et al. [2012] for ^{14}C, Masarik and Beer [1999, 2009] for both cosmogenic isotopes). Because our carbon cycle model is similar to Bard et al. [1997], we have adopted the same global ^{14}C production rate value (1.72 at.m^{-2}.s^{-1}). Our model was then used to simulate atmospheric $\Delta^{14}C$ changes in response to changing ^{14}C production during the Laschamp event. We focus on the period between 45500 yr BP and 37500 yr BP. A figure with the values of fluxes as well as a table with box volumes and areas are given in Supplementary Material (appendix B).

To examine if our model is coherent with previous studies, we first tested the damping and phasing effect of the model, depending on the frequency of production variations, as shown in Fig. 3.5. For this, we have used sinusoidal changes of cosmogenic production as a model input. The frequencies used run from 5 years

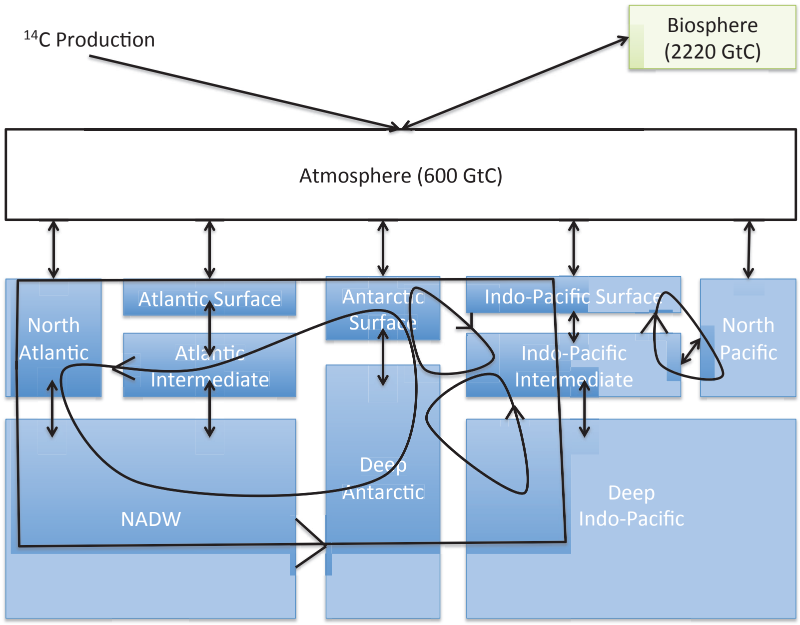

Figure 3.4: Scheme representing our 12-box model (10 ocean boxes + one atmosphere and biosphere box).

to 105 years. The attenuation effect is such that variations in ^{14}C production are attenuated by a factor ~100 for decadal cycles, ~20 for centennial scales and 10 for millennial cycles (see top of Fig. 3.5). This is coherent with other models [Delaygue and Bard, 2011]. Note that the atmosphere in the model is well-mixed, without separation of the troposphere and the stratosphere, which affects the results for periods under 30 years [Siegenthaler et al., 1980]. The other effect of the carbon cycle is the delay between atmospheric ^{14}C concentration and variations in production, expressed as a phase lag in Fig. 3.5. For example, century scale periodicities are shifted by a few decades (bottom of Fig. 3.5). The phase lag of the model is coherent with values presented in Delaygue and Bard [2011].

3.2.5 Simulations of the carbon cycle

With this model, it is possible to have an idea of the impact of the geomagnetic and solar modulations on atmospheric ^{14}C/C. It is interesting to examine effects of changes in the carbon cycle too, because the Laschamp excursion occurred during a glacial period but straddled DO-10 (Dansgaard-Oeschger) interstadial. Several simulations were made with different carbon cycle boundary conditions. The first one (which we call S1) corresponds to the modern preindustrial boundary conditions (light colored curves in Fig. 3.6). The simulation S2 is similar but with the

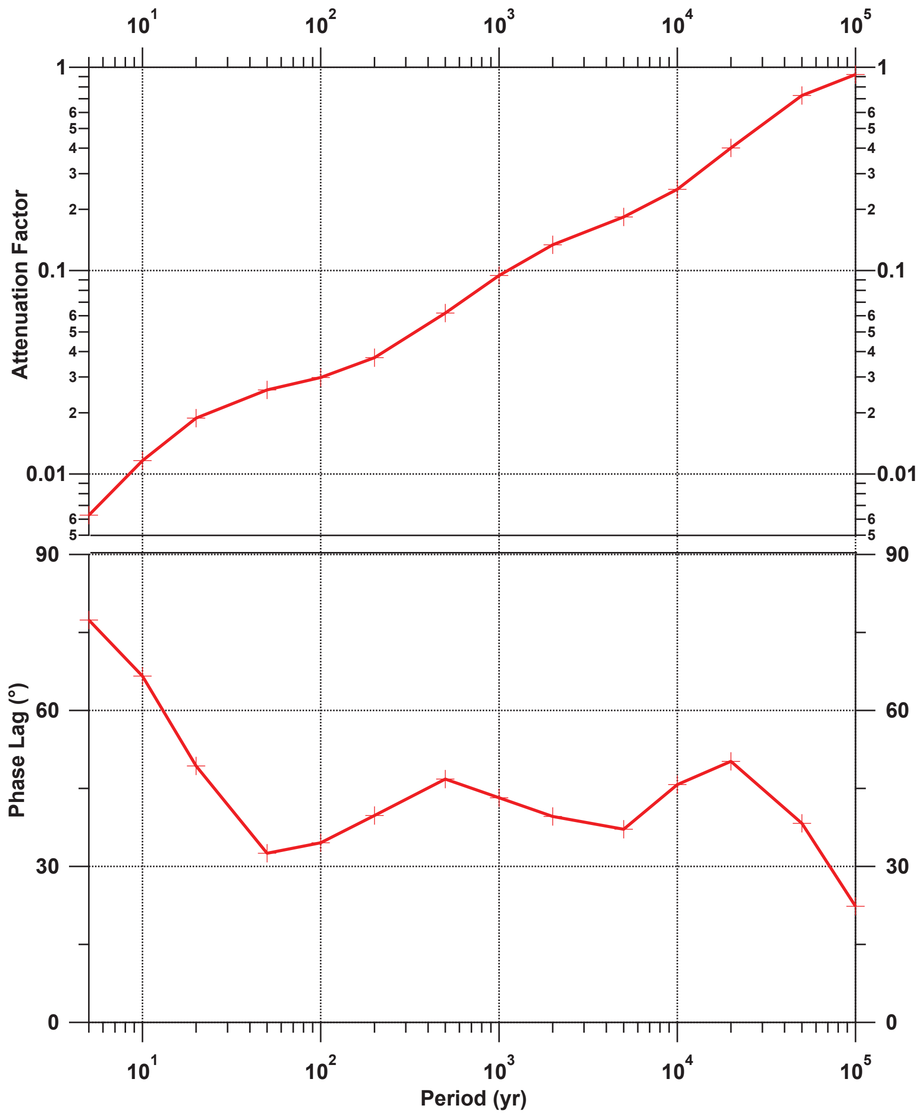

Figure 3.5: Simulated attenuation factor (top) and phase lag (bottom) of atmospheric ratio $^{14}C/C$ for sinusoidal variations in ^{14}C production, as a function of the period of these variations. The attenuation factor is normalized to the size of the production change. The phase lag is calculated as the time lag divided by the period and multiplied by 360°.

atmosphere and terrestrial biosphere reduced to respectively 75% and 65% of their preindustrial carbon inventories [Indermühle et al., 2000; Hughen et al., 2004]. The results of this simulation are plain colored in Fig. 3.6. For the third simulation (called S3), we added a reduction of the North Atlantic Deep Water (NADW) fluxes by 1/3 [Laj et al., 2002; Hughen et al., 2004] to simulate estimated glacial conditions (dark colored curves in Fig. 3.6). The system is initialized at an equilibrium state before the beginning of the simulation.

3.3 Results from ^{10}Be flux records

Here we discuss Δ^{14}C variations inferred from ^{10}Be-based production rate, using calculations from Masarik and Beer [2009] and KOV simulation [Kovaltsov and Usoskin, 2010; Kovaltsov et al., 2012], with the different scenarios presented in section 3.2.5. The results are presented in section 3.3.1 for EPICA Dome C (Antarctica) and in section 3.3.2 for the composite ^{10}Be record from Greenland. All graphs are brought together in Fig. 3.6. The results using Masarik and Beer [2009] formulas and KOV calculations are in red and green respectively. Moreover, we compare our results from assumed glacial conditions (S3) with Δ^{14}C from IntCal09 calibration curve in section 3.3.3 [Reimer et al., 2009].

3.3.1 EPICA Dome C

The resulting Δ^{14}C from the EDC input with the calculations of Masarik and Beer [2009] and KOV [Kovaltsov and Usoskin, 2010; Kovaltsov et al., 2012] are shown on Fig. 3.6a under the different scenarios. Concerning the results using Masarik and Beer [2009], atmospheric Δ^{14}C increases by 400‰ using the modern case simulation S1 (light red). Applying simulations S2 and S3 (plain and dark red curves, see section 3.2.5), gives relatively minor changes on atmospheric Δ^{14}C (amplitude of 410‰ with simulation S2 and 430‰ with simulation S3). Using KOV calculations, we obtain amplitudes of 235‰, 250‰ and 260‰ with scenarios S1, S2 and S3 respectively. We can see that the difference of sensitivity between the simulations of ^{10}Be and ^{14}C production (see Fig. 3.2, Masarik and Beer [2009]; Kovaltsov and Usoskin [2010]; Kovaltsov et al. [2012]) leads to very different results in the modelled atmospheric Δ^{14}C from ^{10}Be records (see section 3.4.1). By contrast, the changes due to the choice of parameters of the carbon cycle model do not seem to influence the results greatly.

3.3.2 Greenland

The results for the Greenland composite record are presented in Fig. 3.6b. Applying the modern simulation S1 and Masarik and Beer [2009] formulation, the modelled atmospheric Δ^{14}C increases by 475‰. With simulations S2 and S3, atmospheric Δ^{14}C increases only slightly (+10‰ and +35‰ for scenario S2 and S3 respectively). Using KOV conversion, the variability between the three scenarios is lower with amplitudes of 295‰, 310‰ and 320‰. Note that for the same scenario and calculation, the amplitudes of atmospheric Δ^{14}C obtained with Greenland input are higher than with EDC input.

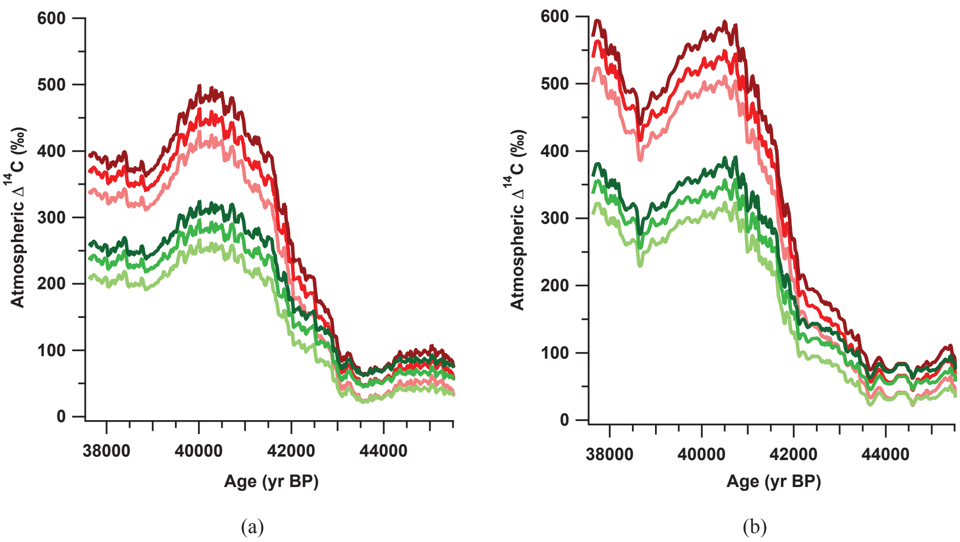

Figure 3.6: Relative variations in atmospheric ^{14}C content simulated by applying the ^{10}Be-based ^{14}C production for (a) EPICA Dome C (Antarctica) and (b) Greenland. Light curves correspond to pre-industrial conditions (S1), plain curves to reduced carbon inventories of atmosphere and biosphere (S2), and dark curves to glacial conditions (S3 = S2 + reduction of NADW formation). Red and green curves represent atmospheric Δ^{14}C variations using ^{10}Be – ^{14}C conversion from Masarik and Beer [2009] and KOV [Kovaltsov and Usoskin, 2010; Kovaltsov et al., 2012] respectively.

3.3.3 Comparison with IntCal09

We compare here our results under assumed glacial conditions (S3) with Δ^{14}C from the IntCal09 calibration curve [Reimer et al., 2009]. This comparison is shown in Fig. 3.7. In Fig. 3.7b, simulated Δ^{14}C from ^{10}Be EDC (light) and Greenland (dark) records have been shifted by +195‰ in order to make the initial conditions similar to the IntCal09 curve. As noted before, results of Δ^{14}C using Masarik and Beer [2009] calculations reach a much higher amplitude than those with KOV values.

The EDC amplitudes are 430‰ and 260‰ (section 3.3.1), while the amplitudes of $\Delta^{14}C$ with Greenland input are 510‰ and 320‰ (section 3.3.2) according to the model applied for the conversion. As for $\Delta^{14}C$ from the IntCal09 curve, it varies around 400‰ between 37.5 and 45.5 ky BP (Fig. 3.7b). We can conclude that results using Masarik and Beer [2009] conversion with ^{10}Be flux seems to be in better agreement with $\Delta^{14}C$ amplitude from IntCal09. $\Delta^{14}C$ with KOV calculations are much smaller. Several differences can be seen in comparison to the IntCal09 curve. Firstly, $\Delta^{14}C$ from IntCal09 is higher on the absolute scale than the results obtained from ^{10}Be flux (Fig. 3.7a), especially comparing with results using the KOV values. The second peak after the Laschamp excursion (around 38.5 ky BP) on the IntCal09 curve is also present on Greenland output (but delayed) but not on $\Delta^{14}C$ from EDC record. However, the most dramatic difference between our calculations and IntCal09 is the much steeper increase at the beginning of the Laschamp event. This increase takes about 3,000 years in our calculations, and about twice as long in IntCal09. This might be explained by a variable carbon cycle not taken into account in our calculations, or the uncertainties of ^{14}C calibration during this period.

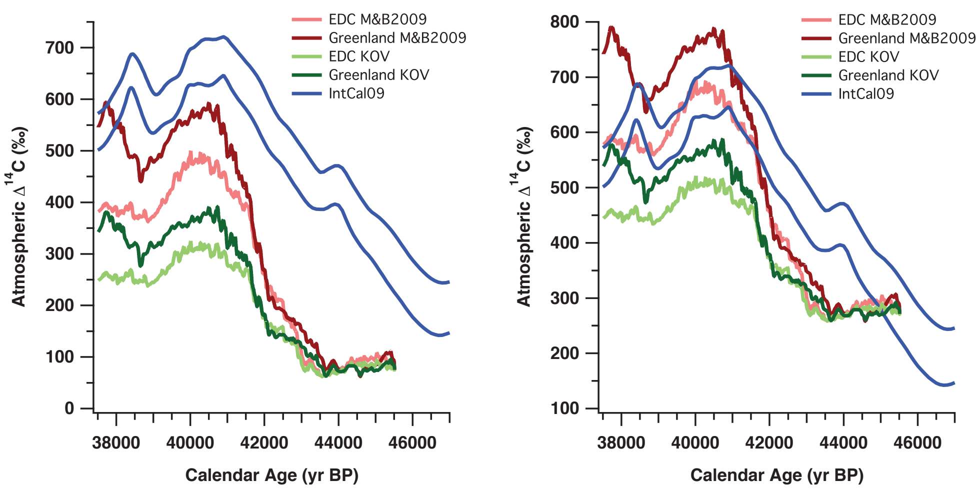

(a)

(b)

Figure 3.7: Comparison of $\Delta^{14}C$ from our simulations with scenario S3 with $\Delta^{14}C$ from IntCal09 calibration curve [Reimer et al., 2009]. $\Delta^{14}C$ from ^{10}Be records are on their absolute scale on graph (a) and shifted by +195‰ on graph (b) to focus on the amplitude of the signals. The light and dark curves represent simulated atmospheric $\Delta^{14}C$ using the EDC and Greenland records respectively. The red and green curves always symbolize $\Delta^{14}C$ variations using ^{10}Be – ^{14}C conversion from Masarik and Beer [2009] and KOV [Kovaltsov and Usoskin, 2010; Kovaltsov et al., 2012] respectively. $\Delta^{14}C$ from IntCal09 calibration curve [Reimer et al., 2009] is shown within its 1-standard deviation envelope (blue curve).

3.4 Discussion

One of the initial motivations of this study was to see whether the increased sensitivity of cosmogenic isotope production to solar modulation during periods of low geomagnetic intensity could lead to significant fluctuations of ^{14}C during the Laschamp event. As can be seen in Fig. 3.6–3.8 and the simulated calibration curve (Fig. S2 in Supp. Mat.), while there are fluctuations as large as 30‰, and predicted reversals over a period of several hundred years, these effects are not dramatic. This is due to the strong damping effect of the carbon cycle on centennial production variations. The results obtained with the help of our simple box-model and presented in section 3.3 confirm several points: (i) the changes of boundary conditions on the carbon cycle do not significantly influence the resulting amplitudes of $\Delta^{14}C$, (ii) for the same scenario and calculation, the $\Delta^{14}C$ amplitude from EDC is lower than the one from the composite Greenland record (between 60‰ and 80‰ of difference), due perhaps to the aspects discussed in section 3.2.1, (iii) the formula used for ^{10}Be – ^{14}C conversion has huge consequences on simulated $\Delta^{14}C$ (see section 3.4.1). So we will focus on this last aspect, especially the difference between cosmogenic isotope productions simulated by Masarik and Beer [1999], their update of 2009 and the KOV model [Kovaltsov and Usoskin, 2010; Kovaltsov et al., 2012]. The possible uncertainties due to carbon cycle changes will also be mentioned.

3.4.1 Sensitivity of ^{10}Be – ^{14}C conversion

The conversion of ^{10}Be (or geomagnetic paleointensity) into ^{14}C is certainly the most important point in atmospheric ^{14}C modeling (as shown in section 3.2.3). Different formulations of global ^{10}Be and ^{14}C production rate as a function of geomagnetic field intensity are presented on Fig. 3.2a. For the geomagnetic intensity $B = 0$ (and the solar modulation $\phi = 550$ MV), global ^{10}Be production rates are equal to 2.07, 1.88 and 2.7 (relative to the present level) with simulation of Masarik and Beer [1999], their update of 2009, and Kovaltsov and Usoskin [2010] calculations respectively. KOV calculations show a considerably stronger dependence for ^{10}Be production on the geomagnetic field intensity than Masarik and Beer [1999, 2009]. As for global ^{14}C production rates, they reach values of 2.38, 2.38 and 2.2 respectively (Kovaltsov et al. [2012] for the last value). Focusing on the variations of $^{14}C/^{10}Be$ global production rate ratio as a function of geomagnetic field intensity (Fig. 3.2b), one may notice that (i) the $^{14}C/^{10}Be$ ratio from KOV [Kovaltsov and Usoskin, 2010; Kovaltsov et al., 2012] is clearly lower (by a factor 2) than the two others (see their respective articles for the absolute value of ^{10}Be and ^{14}C) and (ii) the slopes of ^{14}C/^{10}Be ratios of Masarik and Beer [1999, 2009] and KOV [Kovaltsov and Usoskin, 2010; Kovaltsov et al., 2012] calculations are very different. From B = 1 to B = 0, the ^{14}C/^{10}Be production rate increases by 15% with the Masarik and Beer [1999] simulation, by 26% with their 2009 update and remains constant with the KOV calculations [Kovaltsov and Usoskin, 2010; Kovaltsov et al., 2012], except for B < 0.1, where it decreases. This last point has strong consequence on simulated Δ^{14}C, as shown in Fig. 3.6–3.8. According to J. Beer (private communication), it is the lower energy threshold for the production of ^{14}C which results in the dependence of the ^{14}C/^{10}Be production ratio with geomagnetic field intensity. This seems intuitively reasonable to us. According to I. Usoskin (private communication), this difference in threshold does not lead to such dependence. Comparing the amplitudes of Δ^{14}C obtained with both calculations (in the order Masarik and Beer [2009], and KOV [Kovaltsov and Usoskin, 2010; Kovaltsov et al., 2012] under glacial conditions (S3), we obtain values of 430‰ and 260‰ for EDC (left graph of Fig. 3.8). For the Greenland input, the resulting amplitudes are 510‰ and 320‰ respectively (right graph of Fig. 3.8). The discrepancy on Δ^{14}C amplitude between the two calculations is huge (approximately a factor 1.6). We point out that the use of the one or another production calculation for the ^{10}Be – ^{14}C conversion leads to a different interpretation of the results during periods of weak geomagnetic shielding. To remedy this situation it will be necessary to clarify the relative dependence of ^{10}Be production as a function of geomagnetic field intensity.

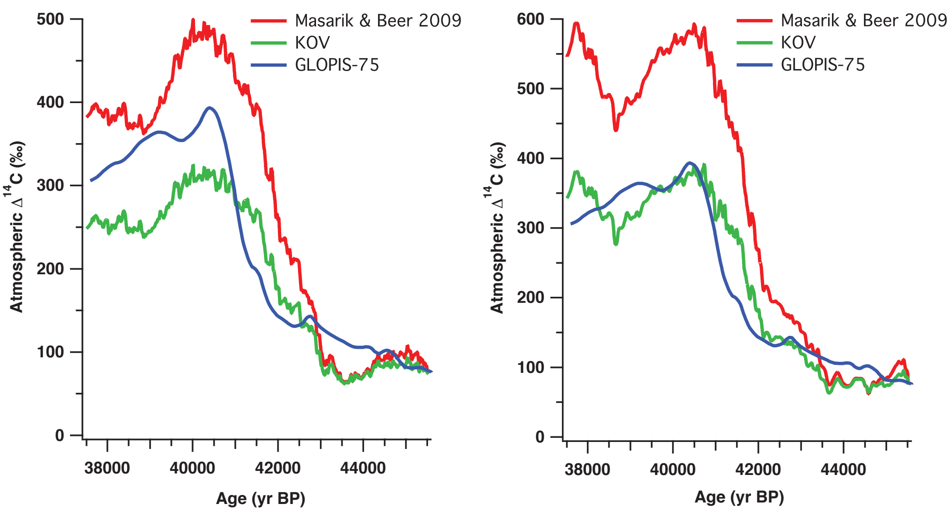

Figure 3.8: Atmospheric Δ^{14}C simulated under glacial conditions using both different production formulations (red: Masarik and Beer [2009], green: Kovaltsov and Usoskin [2010]; Kovaltsov et al. [2012]) with the EDC (left) and Greenland input (right). Δ^{14}C using GLOPIS-75 [Laj et al., 2004] under glacial conditions is also shown (blue).

In contrast to $^{14}C/^{10}Be$, the relative dependence of ^{14}C production on geomagnetic intensity given by Masarik and Beer [2009] and KOV [Kovaltsov et al., 2012] is virtually identical (Fig. 3.2a). This implies that if one assumes the same initial production rate, the two models predict the same ^{14}C response to the Laschamp event, as seen in Fig. 3.3. In Fig. 3.8 we show this response (blue curve) using the same assumed glacial conditions (scenario S3) as used in Figs. 3.6, 3.7, and the geomagnetic field intensity given by GLOPIS-75. One can note several differences compared to that found using ^{10}Be. Most obvious is the absence of the fine structure because the geomagnetic field input lacks the solar modulation variations. Also, because the GLOPIS-75 record of the Laschamp event is significantly shorter than that recorded by ^{10}Be (Fig. 3.1), the resulting ^{14}C peak is narrower than that found using ^{10}Be. Finally, as far as amplitude, that found using GLOPIS-75 is midway between the Masarik and Beer [2009] and KOV results using the ^{10}Be input from EDC, while in very good agreement with KOV using ^{10}Be input from Greenland (Fig. 3.8).

3.4.2 Carbon cycle uncertainties

The conversion of ^{10}Be into ^{14}C is not the only uncertainty of the method we have used. Our lack of knowledge about past changes of the carbon cycle brings also some uncertainties. Indeed, because the Laschamp excursion straddles D–O 10 [Yiou et al., 1997; Raisbeck et al., 2007] 41 000 years ago, the carbon cycle has probably changed during this period, a potential cause of differences between measurements and simulations. For example in our model, it is assumed that oceanic circulation is constant during the experiment between 37.5 and 45.5 ky BP. But in reality, rapid variations of temperature happened, as shown by ice core records [EPICA, 2006], probably leading to changes of oceanic circulation and biosphere (and so carbon cycle). These changes coupled with the Laschamp excursion could modify the $^{14}C/C$ ratio in the atmosphere. Moreover, we began the simulation with a carbon cycle at equilibrium. Depending how the climate (CO_2) changed several thousand years before the period studied, it could influence the resulting atmospheric $\Delta^{14}C$ (release of carbon trapped into deep ocean for example). An on-going work with a more sophisticated dynamical carbon cycle model will focus on the climatic aspects linked to concentration of CO_2 and ocean dynamics.

3.5 Conclusion

Because of their high resolution with a significant structure, ^{10}Be records from EDC and Greenland (GRIP and NGRIP) ice cores are good candidates to study production effects on the amplitude of atmospheric Δ^{14}C during the Laschamp geomagnetic event. Both production calculations from Masarik and Beer [2009] and KOV [Kovaltsov and Usoskin, 2010; Kovaltsov et al., 2012] have been used for the ^{10}Be – ^{14}C conversion, leading to discrepant results. Indeed, atmospheric Δ^{14}C amplitude is different by a factor of 1.6 according to the production calculations applied for the ^{10}Be – ^{14}C conversion. Therefore one must be careful when choosing a production formulation for studying ^{14}C production variations during periods of very low geomagnetic field intensity, such as the Laschamp excursion, using ^{10}Be data. Moreover, we point out the inappropriate use of the approximation from Elsasser [1956] by Hoffmann et al. [2010] for conversion of geomagnetic field intensity into ^{14}C production. It results in a stronger amplitude of atmospheric Δ^{14}C during periods of weak geomagnetic shielding (as the Laschamp event) compared to model calculations. Because of the simultaneity of the Laschamp excursion with D–O event 10 and variations of CO_2 concentration in the atmosphere before the studied period, possible climate effects should be analyzed with the help of a dynamical model. Improved understanding of carbon cycle during the glacial period is required too.

Acknowledgements

We thank I. Usoskin for providing ^{14}C table before it was published and for his prompt replies to our questions. We thank J. Masarik and J. Beer for providing numerical values of their calculations and comments regarding their interpretation. We also want to thank C. Laj and C. Kissel for GLOPIS-75 data, and E. Michel for her useful comments on the model.